Influence of SiO_2 and Al_2O_3 Fillers on Thermal and Dielectric Properties of Barium Zinc Borate Glass Microcomposites for Barrier Rib of Plasma Display Panels (PDPs)

Shiv Prakash Singh, Karan Pal, Anal Tarafder, Tarak Hazra and Basudeb Karmakar*

Glass Technology Laboratory, Glass Division, Central Glass and Ceramic Research Institute (Council of Scientific and Industrial Research), 196. Raja S.C. Mullick Road, Kolkata 700 032, India

Abstract

In a lead-free low temperature sinterable multicomponent barium zinc borate glass system, BaO-ZnO-B_2O_3-SiO_2-Li_2O-Na_2O (BZBSLN), the influence of SiO_2 (amorphous) and Al_2O_3 (crystalline, alpha alumina) ceramic fillers on the softening point (T_s), glass transition temperature (T_g), coefficient of thermal expansion (CTE), and dielectric constant (ε_r) has been investigated with a view to its use as the barrier ribs of plasma display panels (PDPs). The interaction of fillers with glass which occurred during sintering at 570^{o}C has also been studied by XRD and FTIR spectroscopic analyses. It is observed that the filler has partially dissolved in the glass at the sintering temperature leaving some residual filler which results in ceramic-glass microcomposites. The distribution of fillers in the glass matrix and microstructures of the composites have been analyzed by SEM images. It is seen that the T_s, T_g, CTE and ϵ_r are slightly increased as the increase of Al_2O_3 content. While in the case of SiO_2 filler, the T_s and T_g gradually increase whereas CTE and ϵ_r gradually decrease along the addition of SiO_2 increases. These experimentally measured properties have also been compared with those theoretically predicted

values. Both the experimental and theoretical predictions of these properties with added filler contents have been found to be correlated very well. In consideration of the desired properties of barrier rib of PDPs with respect to use on PD200 glass substrates, the addition of Al_2O_3 filler to BZBSLN glass is found to be more preferable than SiO_2 filler.

[Keywords: Plasma display panel, Barium zinc borate glass, Ceramic filler, Thermal properties, Dielectric properties]

---

* Corresponding author; e-mail: basudebk@cgcri.res.in

Introduction

Currently, the application of plasma display panels (PDPs)[1-5] is increasing due to its high quality picture, wide view angle and big screen size which can be hanged on wall. In plasma display panels, components such as transparent dielectric layer, white back dielectric layer, barrier rib etc. are made up of low melting glasses and their microcomposites. Barrier ribs are used as partitions between the red-green-blue (RGB) phosphors cavities to prevent optical cross-talk (i.e., color from one pixel leaking into an adjacent pixel). They are placed between transparent dielectric and white back. Presently various glass powders such as PbO-ZnO-B_2O_3 and PbO-ZnO-SiO_2 are being used for barrier rib which contain huge amount (60-80%) of lead oxide (PbO)[6]. Lead is used in glasses due to its low melting temperature and property tailoring ability. But lead is creating hazardous effect on health and environment. So recently, interest in lead free glass system has greatly been increased with regard to its application to barrier ribs in plasma display panels (PDPs) as an alternative to the currently used lead based glasses. Several requirements such as low softening point, T_s (below 580^{o}C), low glass transition temperature, T_g (below 500^{o}C), comparable coefficient of thermal expansion, CTE (below 90 x 10^{-7}/K) and low dielectric constant, ε_r (8 - 15), which are close to that of PDP glass substrate (PD 200), should be satisfied in order to develop suitable barrier ribs for PDP application. BaO-ZnO-B_2O_3-SiO_2 (BZBS) and BaO-ZnO-B_2O_3 (BZB) glass systems have been reported as alternatives[7-11] for barrier ribs of PDP. Recently, Chong et al[12, 13] have reported the BaO-ZnO-B_2O_3-P_2O_5 glass system for the same.

For fabrication of barrier ribs, in general, crystalline ceramic fillers are also added to form a ceramic particulate-glass microcomposite to modify the softening point, glass

transition temperature, coefficient of thermal expansion and dielectric constant. It is observed that multicomponent glasses yield better performance with respect to PDP application. For this reason, we have selected a multicomponent barium zinc borate, $BaO\text{-}ZnO\text{-}B_2O_3\text{-}SiO_2\text{-}Li_2O\text{-}Na_2O$ (BZBSLN) glass for barrier ribs and investigated its ability to form microcomposites with various types of fillers. The types of filler investigated in this work were SiO_2 and Al_2O_3 for adjustment of various thermal and dielectric properties as well as improvement of mechanical strength. As we aware, this work has not been reported previously. In order to enable the glass matrix to host various types of refractory ceramic fillers (i.e. SiO_2 and Al_2O_3), it is important during the development of the composites that sintering be conducted at a 570^oC, with a strong interfacial bond between the filler and matrix.

In this study, effects of different amount (5 to 20 wt.%) of SiO_2 (amorphous) and Al_2O_3 (crystalline, corundum) on $BaO\text{-}ZnO\text{-}B_2O_3\text{-}SiO_2\text{-}Li_2O\text{-}Na_2O$ (BZBSLN) glass on the resultant softening point (T_s), glass transition temperature (T_g), coefficient of thermal expansion (CTE) and dielectric constant (ε_r) were investigated and compared with theoretically predicted values. The glass-filler interaction has been studied by XRD, FTIR spectroscopy and SEM micrograph analyses.

.

Experimental Procedure

Preparation of Glass and Microcomposite

The batch of the $BaO\text{-}ZnO\text{-}B_2O_3\text{-}SiO_2\text{-}Li_2O\text{-}Na_2O$ (BZBSLN) glass was prepared by using the high purity raw materials such as BaO (GR, 99%, Merck) and ZnO (GR, 99%, Loba Chemie), H_3BO_3 (GR, 99.5%, Loba Chemie), SiO_2 (Quartz) Li_2CO_3

(GR, 99%, Loba Chemie) and Na_2CO_3 (GR, 99%, Loba Chemie). About 500 g glass was melted in a platinum crucible in an electrically heated raising hearth furnace at 1150^oC for 2h in air with intermittent stirring. The molten glass was quenched by casting into an iron plate. The quenched glass was initially crushed in a stainless steel mortar and then pulverized in a planetary mono mill (Retzch, Model PM100) using zirconia jar and ball to obtain final glass powders of 10.1 μm size (d_{50}).

The pulverized BZBSLN glass powders were mixed well in isopropanol medium with appropriate amount of amorphous microsilica, SiO_2 (Pooja Enterprises, 99.5 %, d_{50} = 1.5 μm) and alpha alumina, Al_2O_3 (Alcoa, 99.9 %, d_{50} = 2.0 μm) fillers in an agate mortar. All the powders were then granulated using 2 wt% aqueous solution of polyvinyl alcohol (PVA) followed by pressing uniaxially into disk or cylindrical shape of desired sizes under a pressure of 500 kgf/cm^2 and then dried. It was sintered at 570^oC for 2h in air for measurement of CTE, T_g, ϵ_r, XRD, FTIR spectra and SEM micrographs analyses. The compositions of composites are enlisted in Table I.

Characterization Technique

The particle size distribution was measured by a Malvern Instrument (Mastersizer 2000). The softening point (T_s) of the dried disk was measured by a glass softening point system (Harrop/Labino, Model SP-3A) with an accuracy of $\pm$1^oC. The instrument was previously calibrated with a NBS (National Bureau of Standards, USA) standard glass of known softening point. The CTE and T_g of the sintered microcomposite cylinders were measured with an accuracy of $\pm$0.2% using a horizontal-loading dilatometer (Netzsch, Model 402C) after calibration with standard alumina supplied with the instrument by the

manufacturer. The CTE in the temperature range 50-350^{o}C is reported here. The dielectric constant was measured with an accuracy of $\pm$0.5% at a frequency of 1MHz using a LCR meter (Hioki, Model 3532-50 LCR Hitester) at 25^{o}C. The instrument was calibrated previously by Suprasil-W silica glass (ε_r = 3.8). XRD data of powder samples were recorded using XPERTPRO diffractometer with 2θ varying from 10^{o} to 80^{o} using Ni filtered CuKα (λ = 1.5406 Å) at 25^{o}C, generator power of 45 KV and 35 mA. FTIR spectra were recorded by dispersing the sintered glass and composite powders in KBr with a Perkin-Elmer FTIR spectrometer (Model 1615) at a resolution of $\pm$ 2 cm^{-1} after 16 scans. It was calibrated with a polystyrene film supplied by the instrument manufacturer. The SEM images of the samples were carried out in LEO S430i instrument at 15 kV. The samples were examined after Au coating on the surface to pass the electron beam through it.

Glass properties such as Littleton softening point (T_{Lt}), CTE and T_g were theoretically calculated (predicted) using SciGlass (Glass Properties Information System, Version 6.7) software following the Priven-2000 method[14-17] and dielectric constant by the method of Kharjuzov and Zorin[17].

Results and Discussion

Particle Size Distribution

The extent of interaction of glass and filler at the sintering temperature is largely depended on their particle size and its distribution. Thus, the particle size distribution of BZBSLN glass powder, SiO_2 and Al_2O_3 fillers are measured and shown in Fig.1. It is seen that SiO_2 and BZBSLN powders exhibit bimodal and Al_2O_3 powder monomodal

particle size distributions. The median particle sizes (d_{50}) of BZBSLN glass powder, SiO_2 and Al_2O_3 fillers are found to be 10.1, 1.5 and 2.0 μm respectively. The respective specific surface areas of glass and fillers SiO_2 and Al_2O_3 are 1.51, 5.23 and 3.51 m^2/g respectively.

XRD Analysis

The fillers of SiO_2 and Al_2O_3 react with glass during firing at 570^oC are the fundamental to the formation of filler reinforced glass microcomposites. Thus, they have been examined by XRD analysis. The variation of XRD pattern of microcomposites with added Al_2O_3 filler content is shown in Fig. 2. XRD pattern of alpha alumina is also shown in Fig. 2, curve f for comparison. BZBSLN glass is X-ray amorphous (Fig. 2, curve a). Since the added SiO_2 filler is amorphous, so all the SiO_2 containing microcomposites found to be X-ray amorphous and do not exhibit any characteristic XRD peak (not shown here). On the other hand, Al_2O_3 filler is crystalline, alpha alumina (see Fig. 2, curve f), so the Al_2O_3 containing microcomposites exhibit gradual development of XRD pattern of alpha alumina, Al_2O_3 (JCPDS card No.: 43-1484) with suppressed amorphous character of the resultant microcomposites. XRD patterns clearly depict that the filler has partially dissolved in glass during sintering leaving behind some residual filler in the glass matrix. This observation correlates well with those of FTIR spectral study as discussed later (see section 3.3). Thus, it is clear from XRD analysis that SiO_2 (amorphous) and Al_2O_3 (crystalline) filler containing microcomposites are of amorphous-in-amorphous and crystal (ceramic)-in-amorphous characteristics respectively.

FTIR Spectra Analysis

The FTIR spectra of SiO_2 and Al_2O_3 containing microcomposites are depicted in Figs. 3 and 4 respectively. The FTIR spectra of added filler SiO_2 and Al_2O_3 are also shown therein for comparison. Their IR band positions along with assignments are provided in Tables II and III respectively. The BZBSLN glass has exhibits bands around 1362 and 1231 cm^{-1} for asymmetric stretching vibrations of B-O-B bond and B-O-Si bond respectively and the band around 969 cm^{-1} for symmetric stretching vibration of B-O-B bond of $[BO_4]$ tetrahedral units[18-20]. The band around 650 cm^{-1} is attributed to bending vibration of B-O-B bond whereas the band around 560 cm^{-1} is for bending vibration of B-O-Si bond.

The bands at 1115, 815 and 469 cm^{-1} of SiO_2 filler are attributed for asymmetric stretching vibration of Si-O-Si bond, symmetric stretching vibration of O-Si-O bond and bending vibration of Si-O-Si bond of $[SiO_4]$ tetrahedral unit respectively[18]. After addition of SiO_2 filler (5-20 wt.%) into the BZBSLN glass matrix the characteristic bands of SiO_2 are gradually developed in the microcomposites is around at 1115 and 469 cm^{-1} which indicate the interaction of SiO_2 filler with the BZBSLN glass. The intensity of band around at 1362 cm^{-1} gradually becomes weak as SiO_2 content increases, it again supports the strong filler-glass interaction and the formation of Si-O-B bond.

The alumina filler exhibits doublet bands around 646 and 615 cm^{-1} for asymmetric and symmetric stretching vibrations of Al-O-Al bond of $[AlO_6]$ octahedral unit[21-23] respectively. Whereas its band at 462 cm^{-1} is due to bending vibration of the Al-O-Al bond. After addition of Al_2O_3 filler to the glass matrix, the bands around 1362 and 1231 cm^{-1} of glass matrix remain almost unaffected and the doublet band of Al-O-Al

bond gradually develop. Where as the band around 650 and 560 cm^{-1} of glass matrix for B-O-B and B-O-Si bonds disappear, which indicates the strong interaction of Al_2O_3 filler with glass and the formation of Al-O-B or Al-O-Si bond which merged into the strong doublet around 646 and 615 cm^{-1}. The gradual intensity increase of this doublet and the band around 462 cm^{-1} with increasing Al_2O_3 filler content clearly indicate partial solubility of filler in the glass matrix.

As the fillers content increases in glass the FTIR spectra become closer to that of filler spectra with some deformation of the BZBSLN glass spectra. This indicates that the filler forms strong bonds in the microcomposites and residual fillers left as such. This facts correlate well with XRD analysis as described earlier.

SEM Photomicrograph Analysis

The microstructure of the composites, sintered at 570^oC with SiO_2 and Al_2O_3 fillers was characterized by SEM photomicrographs. Figure 5 depicts the morphology and distribution of residual SiO_2 and Al_2O_3 fillers in the glass matrix. The sintering of glass frits at such a low temperature means that the glass frits are softened enough to attack crystalline phases of the fillers, which yields the uneven-shaped and increased fluidity for the realignment of the fillers. SEM micrographs also show the cracking of microcomposites and its extent is more in SiO_2 containing sample (GS15) compared to that in Al_2O_3 containing sample (GA15). This is due to CTE mismatching between guest filler (SiO_2) and host glass matrix. Some pores are found in the SEM micrographs which indicate that the density of the sintered microcomposites would be less than that of glass.

Softening Point and Glass Transition Temperature

Figures 6 and 7 shows the softening points (T_s) and glass transition temperature (T_g) of the filler-glass microcomposites for both filler types (i.e. SiO_2 and Al_2O_3) as a function of filler addition from 5 to 20 wt%. In both the cases, softening point increases gradually as the filler content increases. A similar trend is observed in the theoretically predicted Littleton softening point ($T_{Lt.}$) and glass transition temperature as well. However, the experimental values in both the cases are lower than those of theoretical predictions. The difference increases with increasing filler content which indicates the partial solubility of the fillers in the glass matrix as also revealed in XRD and FTIR spectral analysis. The close correlation between the experimental and theoretically calculated softening point and glass transition temperature trends clearly indicates that these properties are additive in nature with respect to the constituting chemical components. This is because of the fact that theoretical calculations of the T_{Lt} and T_g are based on additive mathematical formula[14-16] as shown below.

$$P = \sum_{i=1}^{N} g_{i,p}\, m_i n_i \Big/ \sum_{i=1}^{N} m_i n_i \qquad (1)$$

where P is the property being calculated; i is the index of the oxide; N is the number of types of oxides forming the glass in question; m_i is a molar fraction of the i^{th} oxide; n_i is the number of atoms in the formula of the i^{th} oxide and $g_{i,p}$ is a partial coefficient for the i^{th} oxide.

Some properties of added SiO_2 and Al_2O_3 fillers are provided in Table 4 to explain the increasing trends of T_s and T_g of the microcomposites. It is seen that SiO_2 and Al_2O_3 have high melting points of 1723^oC and 2100^oC respectively. Thus, it is thought

that the increase of T_s and T_g of microcomposites is due to high melting points of SiO_2 and Al_2O_3 fillers originated from high Si-O (1.54) and Al-O (1.89) bond strength.

Coefficient of Thermal Expansion

Comparison of variation of experimental and theoretically predicted coefficient of thermal expansion (CTE) as a function of added SiO_2 and Al_2O_3 fillers is shown in Fig.8. The CTE gradually decreases as SiO_2 filler content increases form 5 to 20 wt%. This trend correlates well with that of theoretical prediction as obtained by following the Eq.1, It is seen from Table IV that SiO_2 filler has very low CTE (5.5×10^{-7}/K) as compared to the glass (79×10^{-7}/K). Therefore, the resultant CTE of the composite decreases gradually. Kim et al.[7, 8] have reported a similar effect for BaO-ZnO-B_2O_3 and BaO-ZnO-B_2O_3-SiO_2 glasses on addition of crystalline SiO_2 (quartz) filler. Whereas the CTE initially decreases (5wt% Al_2O_3) which is due to dissolution of Al_2O_3 in glass as is observed in XRD pattern (see Fig. 2, curve b) and correlates well with theoretical prediction. Beyond 5 wt% Al_2O_3, the CTE increases slightly whereas the theoretical prediction is decreasing trend. This discrepancy is due to partial dissolution of Al_2O_3 filler in glass (see XRD in Fig. 2, curve c-e). This very slight increase in CTE is happened due to almost identical CTE of Al_2O_3 filler (70-80 x 10-7/K) and BZBSLN glass (79x10-7/K). Kim et al.[7] reported a similar trend of CTE for BaO-ZnO-B_2O_3-SiO_2 glass on addition of Al_2O_3 filler.

Dielectric Constant

Dielectric constant (ε_r) of the glass and microcomposites has been evaluated by using the following formula[24]

$$\varepsilon_r = cd/(0.0885\ A) \qquad (2)$$

where c, d and A are capacitance in pico Farad (pF), thickness of glass or composite (in cm) and area of the dielectric (in cm^2) respectively.

The comparison of variation of experimental and theoretically predicted (Kharjuzov and Zorin method[17] dielectric constant as a function of added SiO_2 and Al_2O_3 fillers is shown in Fig. 9. It is seen that the dielectric constant of the composites gradually decreases with increase in SiO_2 filler content. On the other hand, the dielectric constant of composites slightly increases with the Al_2O_3 filler addition. All these trends correlate very well with those theoretical predictions. However, the experimental values are higher than those of theoretical predictions. Results reported by Kim et al.[7-8, 11] for SiO_2 (quartz) filler addition to $BaO\text{-}ZnO\text{-}B_2O_3$ and Al_2O_3 filler addition to $BaO\text{-}ZnO\text{-}B_2O_3\text{-}SiO_2$ glasses are nearly identical. It is seen from Table IV that the dielectric constant of SiO_2 filler is 3.8 which is lower than that of the glass (9.3) whereas the dielectric constant of Al_2O_3 filler is close (9-10) to that of glass. So the resultant dielectric constant of SiO_2 filler added composites gradually decrease whereas it slightly increases in case of Al_2O_3 filler addition as expected.

Conclusions

The effect of SiO_2 and Al_2O_3 ceramic fillers to $BaO\text{-}ZnO\text{-}B_2O_3\text{-}SiO_2\text{-}Li_2O\text{-}Na_2O$ (BZBSLN) glasses on the softening point, glass transition temperature, coefficient of

thermal expansion and dielectric properties of has been investigated from the view point of its application to the lead free barrier rib of plasma display panels. From the XRD data, FTIR spectra analyses and SEM images, it is clear that the added fillers are partially dissolved into the BZBSLN glass matrix to form chemical bond with the glass at the sintering temperature (570^{o}C) and thus the specimen successfully formed ceramic filler particulate-reinforced glass matrix microcomposites. The addition of SiO_2 and Al_2O_3 fillers increases both the softening point and glass transition temperatures. The SiO_2 filler has decreased the dielectric constant of the glass, while the addition of Al_2O_3 filler has slightly increases the dielectric constant of the filler-glass composite. In terms of CTE, only the addition of Al_2O_3 filler could successfully achieve the CTE of the composite (80x 10^{-7} K^{-1}) to match with the currently used PDP glass substrate such as PD 200 glass (83x 10^{-7} K^{-1}). By considering all aspects of the properties, the addition of Al_2O_3 filler of about 10-20 wt% to BZBSLN glass is in general the most desirable of type of filler investigated in the current work. It has yielded a softening point of 569^{o}C-576^{o}C, CTE of 80-78 x 10^{-7} K^{-1} and dielectric constant of 10-9.6, which are very close to those of the currently used PbO-based barrier rib. The close correlation of theoretical predictions and experimental values strongly advocates the additive nature of the physical properties with respect to the chemical constituents of the composites.

Acknowledgements : This research has been supported in part by the NMITLI scheme of CSIR, New Delhi. The authors gratefully thank Dr. H. S. Maiti, Director of the institute for his keen interest and kind permission to publish this paper. They also acknowledge the XRD and Ceramic Membrane Sections of this institute for carrying out the XRD and particle size measurement experiments.

References

1. D. M. Mattox and J. H. Robinsion, *J. Am. Ceram. Soc.,* **80,** 1189-94 (1997).

2. J. –H. Jean, S. –C. Lin and S. –L. Yang, *J. Appl. Phys.,* **34,** L422-25 (1995).

3. G. –H. Hwang, H. –J. Jeon and Y. –S. Kim, *J. Am. Ceram. Soc.*, **85,** 2956-60 (2002).

4. N. Fukushima, H. Oshita and T. Mito, U.S. patent 6417123B1, 2002.

5. B. –H. Jung, D. –K. Lee, S. –H. Sohn and H. –S. Kim, *J. Am. Ceram. Soc.,* **86,** 1202-05 (2002).

6. G. –H. Hwang, W. –Y. Kim, H. –J. Jeon and Y. –S. Kim, *J. Am. Soc.*, **85**, 2961-65 (2006).

7. S. –G. Kim, J. –S. Park, J. –S An, K. S. Hong, H. Shin and H. Kim, *J. Am. Ceram. Soc.* **89,** 902-07 (2006).

8. H. Shin, S. –G. Kim, J. –S. Park, J. –S. An, K. S. Hong and H. Kim, *J. Am. Ceram. Soc.*, **89,** 3258-61 (2006).

9. A. N. Sreeram, R. L. Quinn and A. N. Prabhu, U.S. patent 6140767, 2000.

10. Okunaga, Kiyoyuki, Kitamura, Yoshirou, Gotou, Tatsuya, Ohji, Masahiko, Hadano and Kazuo, U. S. patent 6737373, 2004

11. S. -G. Kim, H. Shin, J. -S. Park, K. S. Hong and H. Kim, *J. Electroceram.*, **15,** 129-34 (2005).

12. E. Chong, S. Hwang, W. Sung, H. Kim and H. Shin, *Int. J. Thermophys.*, DOI 10.1007/s10765-008-0496-8, (2008).

13. E. Chong, S. Hwang, W. Sung and H. Kim, *Int. J. Appl. Ceram. Technol.* **1-7,** DOI: 10.1111/j.1744-7402.2008.02273.x, (2008).

14. A. I. Priven, *Glass Tehnol.*, **45,** 244-54 (2004).

15. A. I. Priven, *Glass Phys. and chem.*, **24,** 67-72 (1998).

16. A. I. Priven and O.V.Mazunin, *Glass Technol.*, **44,** 156-66 (2003).

17. SciGlass (Glass Properties Information System), Version 6.7

18. G. Fuxi, *Optical and Spectroscopic Properties of Glass*, pp. 18-61, Springer-Verlag, Berlin, (1992).

19. E. I. Kamitsos, A. M. Karakassides and D. G. Chryssikos, *Phys. Chem. Glasses,* **91,** 1073-79 (1987).

20. S. G. Motke, S. P. Yowale and S. S. Yawale, Bull. Mater. Sci., **25,** 75-78 (2002).

21. V. L. Burdick and D. E. Day, *J. Am. Ceram. Soc.* **50,** 97-100 (1997).

22. V. A. Kolesova, The Structure of Glass, Vol.2, pp.177, Translated from Russian, Consultants Bureau, New York, (1960).

23. V. Stubican and R. Roy, *Am. Mineral*, **46**, 32-37 (1961).

24. T. K. Dakin, "Insulating Materials-General Properties," pp. 4-117 in: *Standard Handbook for Electrical Engineers*, 13th Edn., eds. D. G. Fink, and H. W. Beaty, McGraw Hill Inc., New York, (1993).

Table I : Composition of BaO-ZnO-B_2O_3-SiO_2-Li_2O-Na_2O (BZBSLN) glass derived microcomposites

Sample Identity	Composition (wt.%)		
	Glass (BZBSLN)	Added SiO_2 filler	Added Al_2O_3 filler
G	100		
GS5	95	5	
GS10	90	10	
GS15	85	15	
GS20	80	20	
GA5	95		5
GA10	90		10
GA15	85		15
GA20	80		20

Table II : IR band position and its assignment in glass, microcomposites and SiO_2 filler

Sample identity / Band position (cm^{-1})						Band assignment
G	GS5	GS10	GS15	GS20	SiO_2 filler	
1362(s,b)	1362(s,b)	1362(s,b)	1362(s,b)	1362(s,b)		B-O-B(as-s)
1231(m,b)	1231(m,b)	1231(m,b)	1215(m,b)	1208(w)		B-O-Si(as-s)
		1100(m)	1100(s)	1115(s)	1115(v,s)	Si-O-Si(as-s), B-O-Si(as-s)
969(b)	969(b)	939(w)	931(w)	915(w)		B-O-B(s-v), B-O-Si(as-s)
					815(s)	O-Si-O(s-s)
650(s)	700(s)	700(s)	700(s)	700(s)		B-O-B (b-v)
560(s)	562(w)	565(w)	570(w)	577(w)		B-O-Si (b-v)
	469(s,b)	469(s)	469(s)	469(s)	477(v,s)	Si-O-Si(b-v)

s = strong, b = broad, m = medium, w = weak, sh = shoulder, v = very
as-s = asymmetric stretching vibration, s-s = symmetric stretching vibration,
s-v = stretching vibration, b-v = bending vibration

Table III : IR band position and assignment in glass, microcomposites and Al_2O_3 filler

Sample identity / Band position (cm^{-1})						Band assignment
G	GA5	GA10	GA15	GA20	Al_2O_3 filler	
1362(s,b)	1362(s,b)	1362(s,b)	1362(s,b)	1362(s,b)		B-O-B(as-s)
1231(m,b)	1231(m,b)	1231(m,b)	1215(m,b)	1208(w)		B-O-Si(as-s)
969(b)	969(b)	969(b)	969(b)	969(b)		B-O-B(s-v), B-O-Si(as-s)
650(s)						B-O-B(b-v)
577(s)						B-O-Si(b-v)
		654(b)	677(b)	646(s,b)	646(s,b)	Al-O-Al(as-v)
	592(b)	600(b)	600(s,b)	608(s,b)	615(s,b)	Al-O-Al(s-v)
	454(m,b)	454(s,b)	462(s)	454(s)	462(s)	Al-O-Al(b-v)

s = strong, b = broad, m = medium, w = weak, sh = shoulder, v = very
as-s = asymmetric stretching vibration, s-s = symmetric stretching vibration,
s-v = stretching vibration, b-v = bending vibration

Table IV : Some properties of added SiO_2 and Al_2O_3 fillers

Filler	Crystallinity	Melting point (^oC)	CTE ($x10^{-7}/K$)	Dielectric constant, ε_r	Si-O or Al-O bond strength, Z/a^*
SiO_2	Amorphous	1723	5.5	3.8	1.54
Al_2O_3	Crystalline (alpha alumina)	2100	70 - 80	9 - 10.1	1.89 (CN6)

* Z = formal charge (valency), a = nuclear distance, CN = coordination number

Figure caption

Fig. 1 - Particle size distribution of multicomponent BZBSLN glass, filler SiO_2 and Al_2O_3 powders

Fig. 2 - Variation of XRD patterns with added Al_2O_3 filler content: (a) glass, G, (b) GA5, (c) GA10, (d) GA15 and (e) GA20 (for composition see Table I). XRD pattern (f) of added Al_2O_3 (alpha alumina) filler is also shown for comparison

Fig. 3 - FTIR spectra of glass and composites: (a) glass, G, (b) GS5, (c) GS10, (d) GS15, (e) GS20 (for composition see Table I). FTIR spectrum (f) of added SiO_2 (amorphous) filler is also shown for comparison

Fig. 4 - FTIR spectra of glass and composites: (a) glass, G, (b) GA5, (c) GA10, (d) GA15, (e) GA20 (for composition see Table I). FTIR spectrum (f) of added Al_2O_3 (alpha alumina) filler is also shown for comparison

Fig. 5 - SEM micrographs of microcomposites (a) GS15 and (b) GA15 showing the distribution of SiO_2 and Al_2O_3 fillers respectively in the glass matrix

Fig. 6 - Comparison of variation of experimental and theoretically predicted softening point temperature as a function of added (a) SiO_2 and (b) Al_2O_3 fillers (for composition see Table I)

Fig. 7 - Comparison of variation of experimental and theoretically predicted glass transition temperature (T_g) as a function of added (a) SiO_2 and (b) Al_2O_3 fillers (for composition see Table I)

Fig. 8 - Comparison of variation of experimental and theoretically predicted coefficient of thermal expansion (CTE) as a function of added (a) SiO_2 and (b) Al_2O_3 fillers (for composition see Table I)

Fig. 9 - Comparison of variation of experimental and theoretically predicted dielectric constant (ε_r) as a function of added (a) SiO_2 and (b) Al_2O_3 fillers (for composition see Table I)

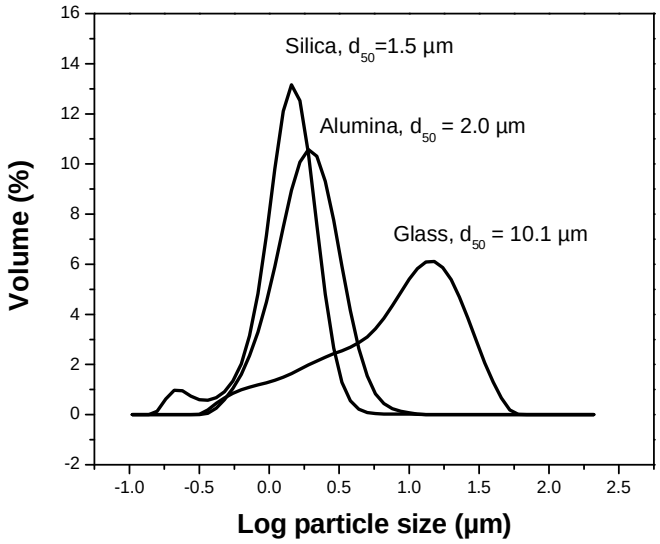

Fig. 1 - Particle size distribution of multicomponent BZBSLN glass, filler SiO_2 and Al_2O_3 powders

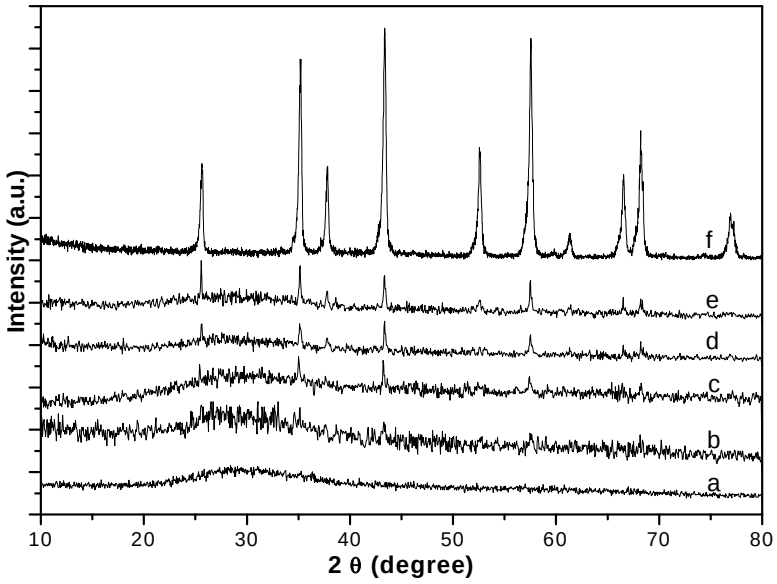

Fig. 2 - Variation of XRD patterns with added Al_2O_3 filler content: (a) glass, G, (b) GA5, (c) GA10, (d) GA15 and (e) GA20 (for composition see Table I). XRD pattern (f) of added Al_2O_3 (alpha alumina) filler is also shown for comparison

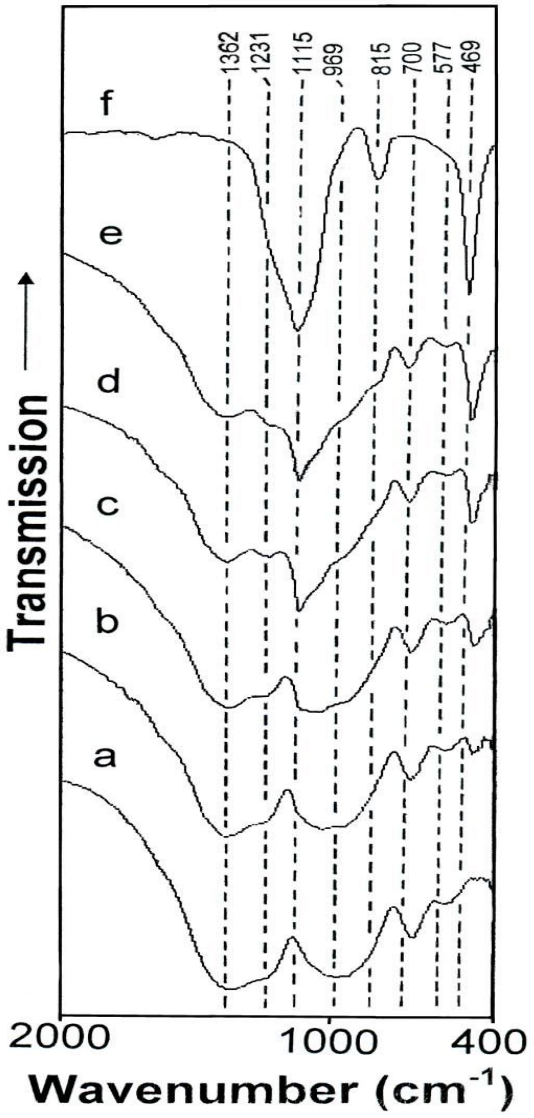

Fig. 3 - FTIR spectra of glass and composites: (a) glass, G, (b) GS5, (c) GS10, (d) GS15, (e) GS20 (for composition see Table I). FTIR spectrum (f) of added SiO_2 (amorphous) filler is also shown for comparison

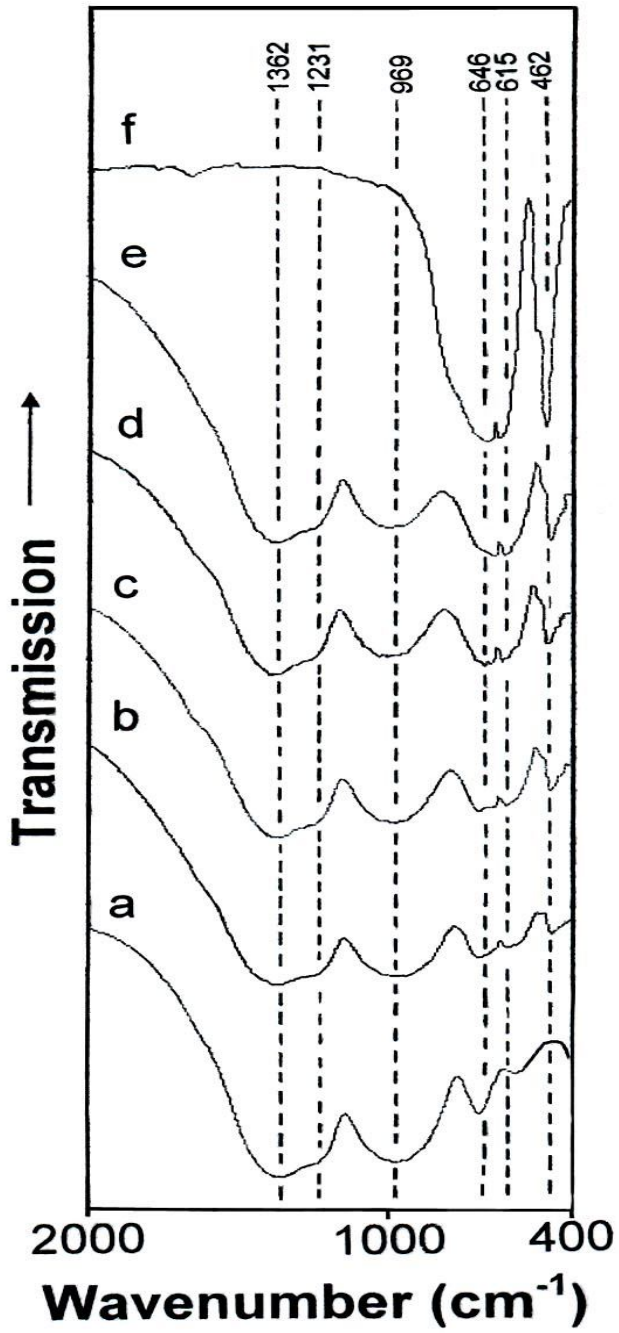

Fig. 4 - FTIR spectra of glass and composites: (a) glass, G, (b) GA5, (c) GA10, (d) GA15, (e) GA20 (for composition see Table I). FTIR spectrum (f) of added Al_2O_3 (alpha alumina) filler is also shown for comparison

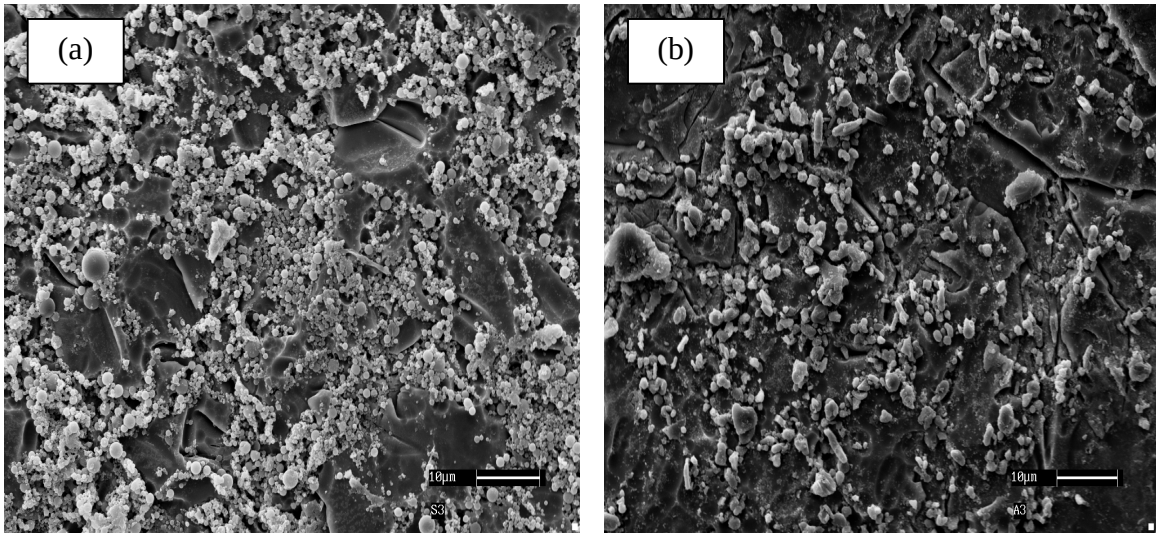

Fig. 5 - SEM micrographs of microcomposites (a) GS15 and (b) GA15 showing the distribution of SiO_2 and Al_2O_3 fillers respectively in the glass matrix

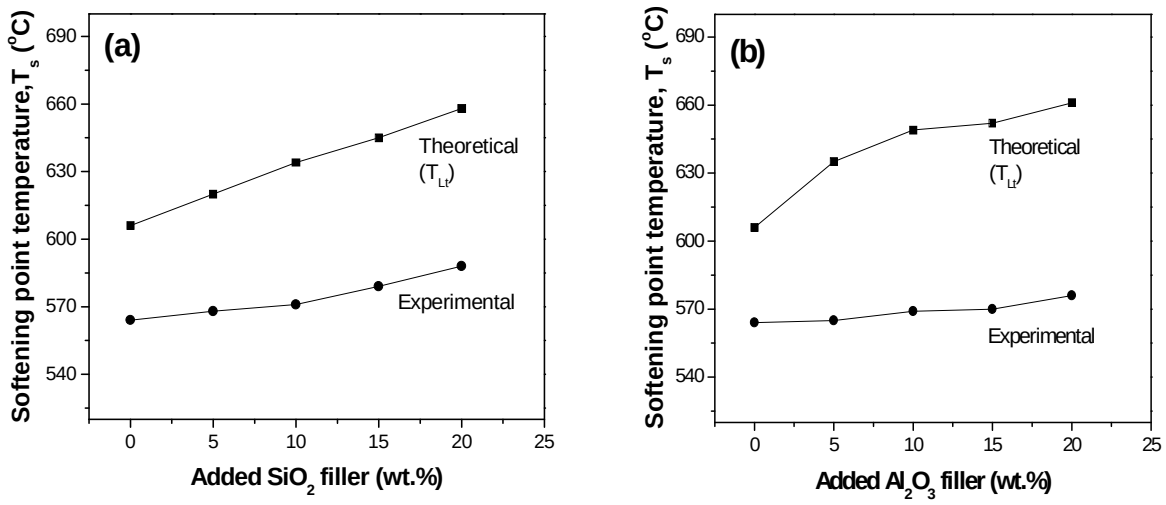

Fig. 6 - Comparison of variation of experimental and theoretically predicted softening point temperature as a function of added (a) SiO_2 and (b) Al_2O_3 fillers (for composition see Table I)

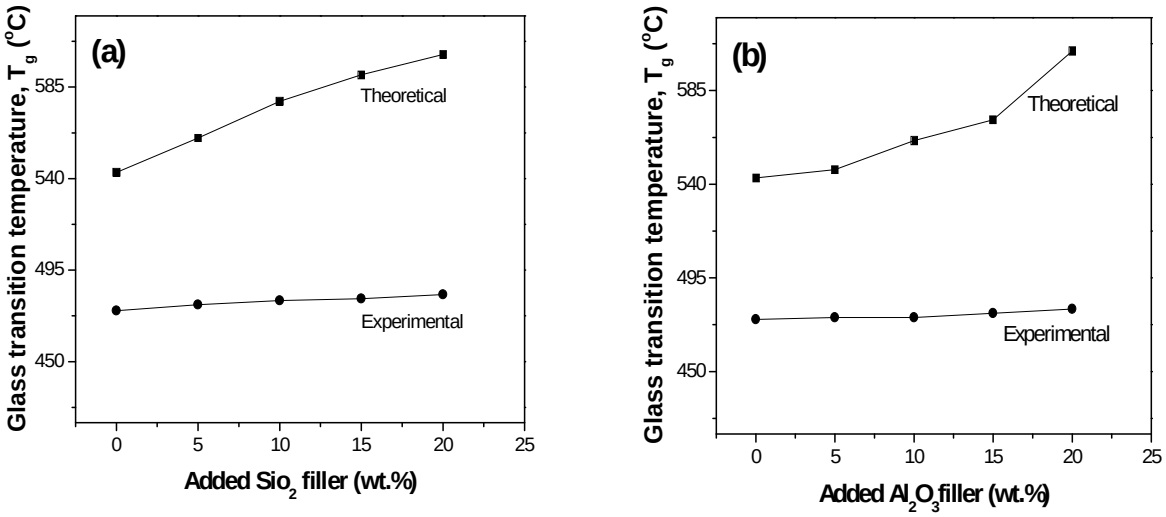

Fig. 7 - Comparison of variation of experimental and theoretically predicted glass transition temperature (T_g) as a function of added (a) SiO_2 and (b) Al_2O_3 fillers (for composition see Table I)

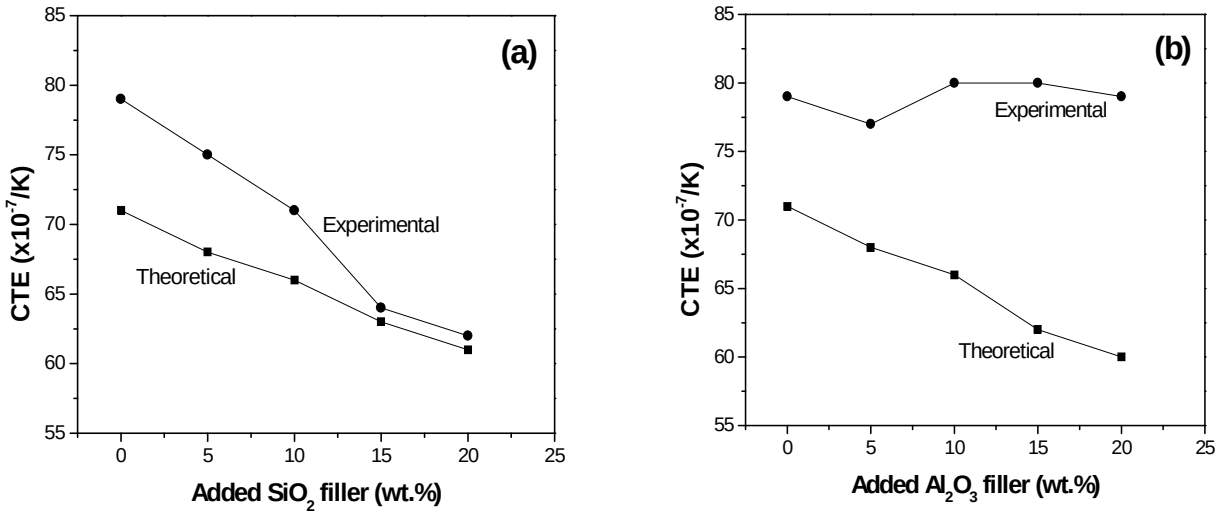

Fig. 8 - Comparison of variation of experimental and theoretically predicted coefficient of thermal expansion (CTE) as a function of added (a) SiO_2 and (b) Al_2O_3 fillers (for composition see Table I)

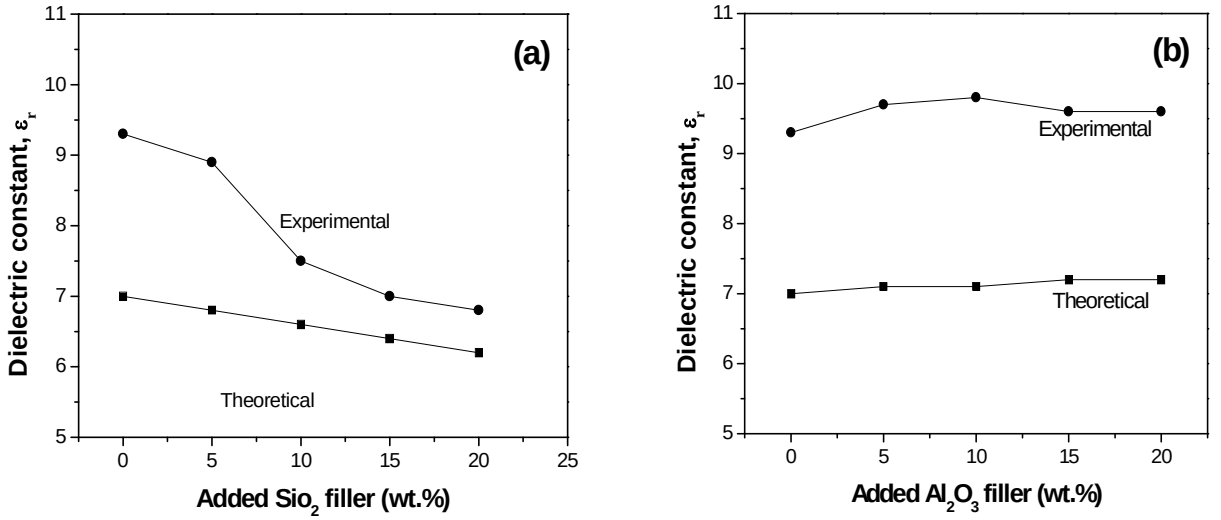

Fig. 9 - Comparison of variation of experimental and theoretically predicted dielectric constant (ε_r) as a function of added (a) SiO_2 and (b) Al_2O_3 fillers (for composition see Table I)